ELSEVIER

Nuclear Instruments and Methods in Physics Research A 446 (2000) 246–252

NUCLEAR INSTRUMENTS & METHODS IN PHYSICS RESEARCH Section A

www.elsevier.nl/locate/nima

The electromagnetic calorimeter of the HERA-B experiment

A. Zoccoli

For the HERA-B Collaboration

Dipartimento di Fisica, Università di Bologna and INFN Via Irnerio, 46, 40126 Bologna, Italy

Abstract

The electromagnetic calorimeter of the HERA-B experiment is described. The main features of the calorimeter calibration procedure are also reported. Finally the first physics signals detected by the calorimeter in recent data taken during the commissioning of the installed HERA-B detector are described.

1. Introduction

HERA-B is a fixed target experiment using an internal target at the 920 GeV proton ring of HERA at DESY in Hamburg/Germany. The main goal of the experiment is to study CP violation in the B system exploiting the *gold-plated* decay mode $B^0 \to J/\psi K_S^0$ which will be identified by detecting the two lepton $J/\psi \to (\mu^+\mu^-/e^+e^-)$ and the $K_S^0 \to \pi^+\pi^-$ decays. The experiment will also cover a wide range of physics topics such as B_S oscillation, rare B-decays, b-*barion* production and c-*quark* physics.

$b\bar{b}$ pairs are produced in the interaction of the proton beam halo with a system of eight wire targets. At this energy the cross-section ratio $\sigma_{b\bar{b}}/\sigma_{inel}$ is of the order of 10^{-6}. Taking into account the *gold-plated* channel branching ratio and reconstruction efficiency, the expected signal to background ratio is expected to be of the order of 10^{-11}–10^{-12}. Therefore to obtain an adequate sample of reconstructed B^0 of O(1000) per year in the interesting final states a constant interaction rate of 40 MHz is required. This corresponds to an average of four inelastic interactions per bunch crossing at the HERA bunch crossing frequency of 10 MHz. A multilevel triggering scheme has therefore been developed in order to achieve high detection efficiency on J/ψ particles and high background rejection. Moreover the detector granularity and the readout and trigger electronics have been designed in order to handle high interaction rates. A detailed description of the apparatus can be found in Refs. [1,2].

We will describe, in this paper, the electromagnetic calorimeter (ECAL) of the experiment and its electronics. We will also outline the used calibration procedure and we will show the results obtained during the first data taking.

2. The electromagnetic calorimeter

The main task the ECAL subsystem is to provide a fast pretrigger signal for the First Level Trigger

E-mail address: zoccoli@bo.infn.it (A. Zoccoli).

0168-9002/00/$ - see front matter
PII: S0168-9002(00)00070-X

(FLT) on electron/positron candidates coming from J/ψ decay. Moreover it must supply position measurements, a good electron–hadron separation, and photon trigger and detection.

To fulfil these requirements a sampling calorimeter of the *shashlik*-type [3] has been designed. The detector is located at ~ 13.5 m distance from the target and is made out of a matrix of 56 columns $\times$ 42 rows of *shashlik* modules. Each calorimeter module is made of a square cross-section tower with 11.19 cm side, where active scintillator layers alternate with the converter ones, all being crossed by optical fibers light guides. The granularity of the detector increases with the decreasing distances from the beam axis, in order to keep the maximum occupancy at a level smaller than 10%. Therefore ECAL has been subdivided into three sections: *Inner, Middle* and *Outer*. In the *Inner* region the converter material is a (W–Ni–Fe) metal alloy, in order to have a small Molière radius (~ 1.3 cm) and the containment depth is ~ 23 radiation length (X_0). In the *Middle* and *Outer* sections, where the track density is low, the converter is lead, the Molière radius is (~ 3.5 cm) and the containment is $\sim 20\, X_0$.

The energy and spatial resolutions for electromagnetic showers reconstructed in ECAL can be written respectively as

$$\frac{\sigma(E)}{E} = \frac{C_1}{\sqrt{E(\mathrm{GeV})}} \oplus C_2,$$

$$\sigma_{X,Y}(\mathrm{cm}) = \frac{D_1}{\sqrt{E(\mathrm{GeV})}} \oplus D_2. \qquad (1)$$

The design values of the constant C_1, C_2, D_1 and D_2 are shown in Table 1.

The ECAL photomultipliers have been chosen in order to cover a wide dynamic range. For the *Inner* region FEU-68 have been chosen, except in the very proximity of the beam line where, due to the high radiation level present in this region, HAMAMATSU-R5600 PMs have been installed. For the *Middle*/*Outer* sections FEU-84-3 PMs are used.

3. The calorimeter electronics

The ECAL read-out and pretrigger electronics have been designed to fulfil the tight experimental requirements in terms of accuracy, speediness, efficiency and flexibility. In particular these electronics provide an early digitization, work with pedestal subtracted data, have a suitable pipeline for the data coming from the front-end, calculate (at the pretrigger level) the physical relevant quantities of an e.m. shower and foresee powerful debugging features.

The ECAL readout system (RO) [4,5] can be divided into two major functional blocks:

- the front-end driver (FED) part divided into 8 ADC sections, each one handles four analog input signals fed by the PMs and performs a fast digitization by means of a 10 MHz 12-bit flash ADC.
- The Digital Logic part processes the digitized signals handling the FLT accepted events and providing suitable interfaces to the VME bus and to the HERA-B DAQ system.

The data generated by each ADC section follow two paths. On one side they are stored into a Dual Port Ram (DPRAM) organized as a circular buffer of 256 events, then, if accepted by the First Level

Table 1
Stochastic and constant terms for the energy and spatial resolutions of the electromagnetic calorimeter of the HERA-B experiment

Module type	Cell size (cm)	C_1 ($\mathrm{GeV}^{1/2}$) (%)	C_2 (%)	D_1 (cm $\mathrm{GeV}^{1/2}$)	D_2 (cm)
Inner	2.2	17	1.6	1.1	0.16
Middle	5.6	9.5	1.0	1.9	0.20
Outer	11.2	9.5	1.0	2.2	0.66

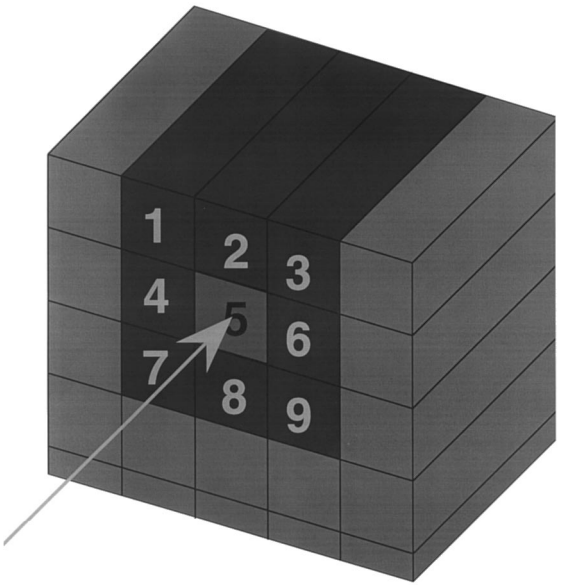

Fig. 1. The nonet of towers used at the pretrigger level to define an ECAL cluster.

Trigger, they are sent to the DAQ system through an Event Buffer. On the other side the data are passed to a Look-Up Table (LUT) that performs the pedestal subtraction, the conversion of the ADC channels into energy and produces a 8 bit digital compressed word for the pretrigger processor. From here these data are sent to the ECAL pretrigger by means of a serial synchronous protocol providing the transmission of one event per each bunch crossing. The ECAL pretrigger (EPT) is an asynchronous system that provides electron/positron candidates to the FLT with a latency of about 3 μs [6].

The measurement of the lepton energy in the ECAL pretrigger is performed by summing up the energies deposited on a nonet of towers (see Fig. 1) and requiring that the following threshold conditions are satisfied:

$$\sum_{i=1}^{9} E_i > E_{\mathrm{TH}}, \quad E_5 > E_{\mathrm{TH}}/2 \tag{2}$$

$$E_{\mathrm{TH}} = K_{\mathrm{TRIG}}\left(\frac{1}{R} + \frac{1}{\sqrt{x^2 + |y^3|}}\right). \tag{3}$$

In these equations E_5 represents the energy deposited in the central tower of the nonet, R is the distance of the tower from the beam axis, x and y are the horizontal and the vertical distances from the beam axis and K_{TRIG} is a constant term (typically $K_{\mathrm{TRIG}} = 550\,\mathrm{GeV\,cm}$). As one can see the threshold depends on the position of the cluster in the ECAL, being the occupancies function of the distance from the beam axis.

Another crucial point of the pretrigger is the capability to perform the center of gravity calculation to determine with high precision the electron impact point on the ECAL, using

$$X_{\mathrm{G}} = \frac{\sum_i E_i X_i}{\sum_i E_i}, \quad Y_G = \frac{\sum_i E_i\, Y_i}{\sum_i E_i} \tag{4}$$

and applying also an S-shape correction. In fact a precise determination of the lepton impact point can reduce significantly the background coming from electromagnetic clusters overlapped to charged tracks. Another original feature of the EPT system is the possibility to recover the electron/positron energy loss via bremsstrahlung, due to the presence of material before the magnet region, thus improving significantly the resolution on the J/ψ reconstruction at the FLT level.

4. The calorimeter calibration

All the ECAL modules, together with the photomultipliers and the Cockroft–Walton bases, the control electronics and a LED pulse system, are installed in the experimental area. The readout and the pretrigger boards are in the final production phase and are being installed immediately as they are delivered.

The detector has taken data continuously since the end of 1998, testing the functionality of the DAQ and the Trigger chains.

One of the crucial items faced in this phase has been the energy calibration of the calorimeter. The final goal is to reach an accuracy in the ECAL calibration at a level of 1% [7]. After detailed studies performed both on Monte Carlo and real events, an iterative calibration procedure based on the π^0 detection has been developed. This choice

gives many advantages, in fact: the π^0 are copiously produced in the inelastic events ($\sim 7\pi^0/ev$ in the target); the gammas from the π^0 decay cover a wide energy spectrum; the signal can be clearly seen; the procedure can be applied without using external information (e.g. from the tracking devices) and can run both at the off-line and on-line modes.

The guidelines of the method are the following: for each event the invariant mass of all possible two-cluster combination is calculated using the equation

$$m_{12} = \sqrt{2E_{\gamma 1}E_{\gamma 2}(1-\cos(\theta_{12}))} \quad (5)$$

where $E_{\gamma 1}$ and $E_{\gamma 2}$ are the measured energies of the two photons and θ_{12} is the decay opening angle. If the cells belonging to the two clusters are not well calibrated m_{12} is shifted with respect to the π^0 nominal mass according to the relation

$$m_{\gamma 1\gamma 2} = \sqrt{2\lambda_1 E_{\gamma 1}\lambda_2 E_{\gamma 2}(1-\cos(\theta_{12}))} = \sqrt{\lambda_1\lambda_2}\cdot m_{12} \quad (6)$$

where the terms λ_i are called calibration factors and are different from the unity if the calorimeter is not perfectly calibrated. The amount of this shift is mainly due to the calibration factors of the central cell of each cluster where most of the energy is deposited. The main steps of the calibration procedure then are the following:

(1) the events undergo the reconstruction;
(2) the invariant mass of all possible two clusters combinations is obtained by Eq. (5) and it is associated to the most energetic cell in each cluster. After collecting enough statistics, it is possible to get an invariant mass distribution containing a pi0 peak for each cell in the calorimeter.
(3) the π^0 peak position of each distribution is evaluated;
(4) the calibration factors are obtained forcing the peaks to the nominal π^0 mass.

The procedure from steps (1)–(4) can be iterated until the obtained calibration factors λ_i are converging to unity.

This method provide a fine tuning of the ECAL calibration but needs starting values for the calibration constants. In the present case these latter have been obtained from occupancy studies.

The reachable precision is bound to the statistics available for each single channel, and the problem can be solved by applying the procedure to groups of cells. A good monitor of the obtained accuracy is the width of the π^0 peak. Extended Monte Carlo simulations show that the detector nominal π^0 resolution ($\sigma_{\pi^0} \sim 7$ MeV/c^2) is worsen to ~ 10 MeV/c^2 for a calibration accuracy of $\sim 5\%$ and to ~ 18 MeV/c^2 for an accuracy of $\sim 20\%$. The flexibility of the method and the minimum amount of information needed for its application allows to run this procedure not only in the offline reconstruction stage, but also online analyzing data coming directly from the Second Level Buffer (SLB) with a consistent reduction of the time allocated for the calibration.

The effectiveness of the calibration procedure can be seen in Fig. 2. The lowest part of the two-cluster invariant mass spectrum is shown for a typical run before (dashed line) and after (continuous line) two iterations of the procedure. As on can see after the calibration the π^0 peak is shifted to the nominal position, its width is consistently reduced and the number of reconstructed π^0 increased. Moreover a peak in the η position appears.

5. The first physics signals

Many engineering runs have been performed in order to test the parts of the detector already installed as well as the DAQ and the trigger capabilities of the experiment. In this paper the results obtained from the analysis of a sample of about 1.2 million of events are described.

The used set-up included about 80% of the *Inner* and *Middle* sections of ECAL instrumented with the readout electronics, three half layers and one complete layer of the Silicon Vertex Detector (SVD), the complete Ring Image Cherenkov detector (RICH) and parts of the Muon detector, of the tracking system and of the Transition Radiation Detector (TRD). Moreover about 10% of the ECAL pretrigger boards were installed.

The signals coming from the ECAL photomultipliers were sent through the front-end drivers to

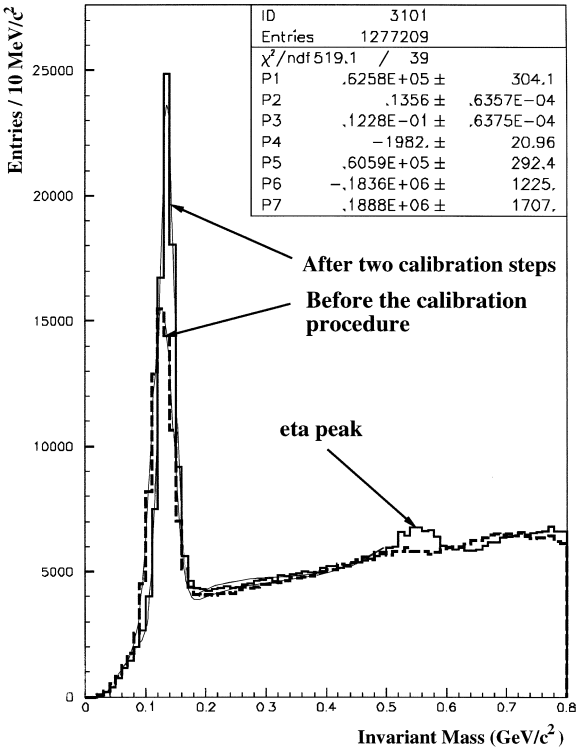

Fig. 2. Results of the π^0 calibration: two-cluster invariant mass distribution before the application of the calibration procedure (dashed line) and after to calibration iteration (continuous line).

the readout system and were processed by the ECAL pretrigger. The cluster candidates passing the pretrigger thresholds were then analyzed by the First and Second Level (SLT) Triggers and eventually sent to the DAQ.

The chosen trigger conditions were the following: at least one ECAL cell with a transverse momentum (P_T) greater than 1 GeV/c in the equipped pretrigger region and at least two clusters on ECAL with $P_T \geq 1.1$ GeV/c and with an invariant mass above 2.2 GeV/c^2. The calibration accuracy was about 5%.

The obtained two-cluster invariant mass distribution is shown in Fig. 3, where each cluster had $P_T \geq 0.4$ GeV/c. A clear π^0 peak containing more than 0.25 million of events is present. The width of the peak is $\sigma = 10.8$ MeV/c^2 ($\sigma(m)/m \sim 8\%$). The η signal is also present.

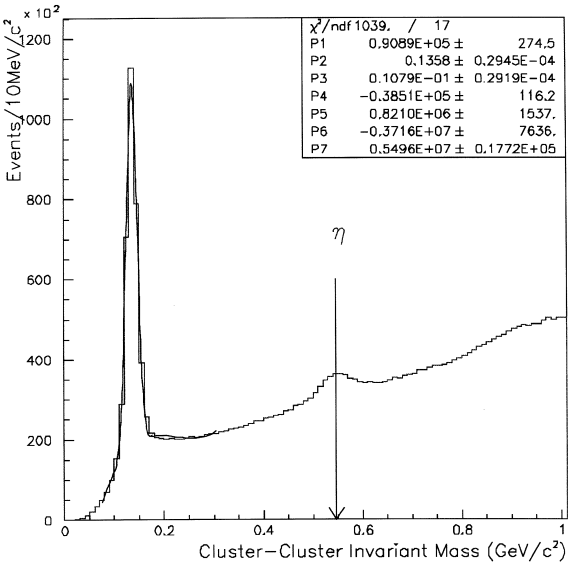

Fig. 3. Two-cluster invariant mass from triggered data requiring both clusters with $P_T > 0.4$ GeV/c.

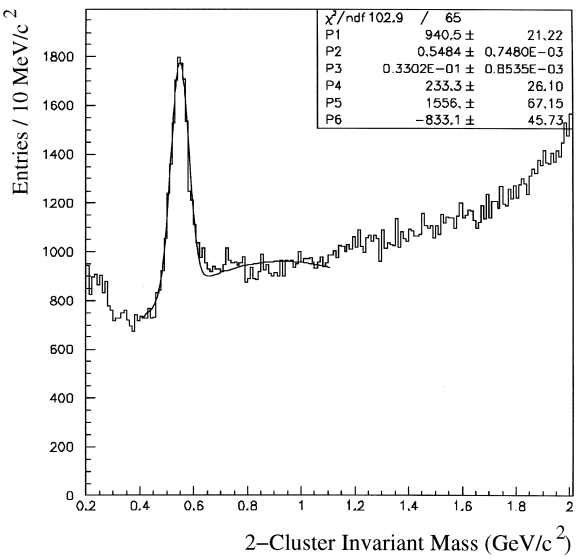

Fig. 4. Two-cluster invariant mass from triggered data requiring both clusters with $P_T > 0.9$ GeV/c.

When we selected events with two clusters with $P_t \geq 0.9$ GeV/c then a very clear η peak appeared (see Fig. 4) showing a width of $\sigma = 33$ MeV/c^2. The

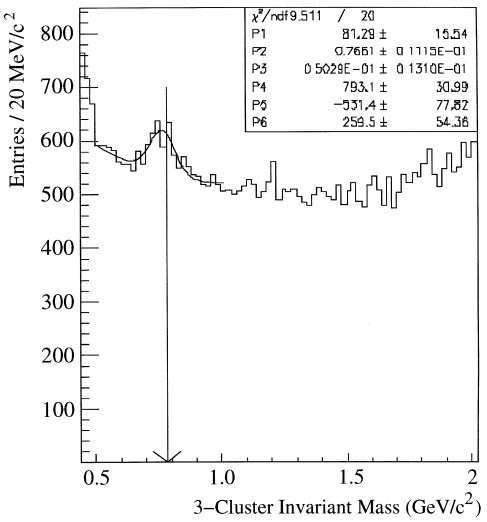

Fig. 5. Three-cluster invariant mass from triggered data, requiring that the invariant mass of a couple is in the π^0 region ($\pm 2\sigma$) and the third cluster with $P_T > 0.9$ GeV/c.

corresponding mass resolution is $\sigma(m)/m \sim 6\%$ and it is a little bit better than the π^0 one as expected.

When we selected three clusters by requiring two clusters with $P_t \geq 0.4$ GeV/c and falling within the π^0 invariant mass region ($\pm 2\sigma$ around the peak) and a third cluster with $P_t > 0.9$ GeV/c we obtained the invariant mass spectrum shown in Fig. 5. A fairly evident ω peak corresponding to the $\omega \to \pi^0\gamma$ decay mode is present. The mass position $m_\omega = 766 \pm 11$ MeV/c^2 is compatible within the error with the nominal value $m_\omega(\mathrm{PDG}) = 781.9$ MeV/c^2 and the width of the peak ($\sigma = 50$ MeV/c^2, $\sigma(m)/m \sim 6\%$) is well in agreement with the expectation.

In order to detect particles or resonances decaying into electrons/positrons, like for example J/ψ, and to reduce at the same time the background coming from photons, information from a tracking device are needed. In the analyzed sample the VDS detector was used in this way. We defined electron/positron candidates requiring hits in a sensitive area centered around the intersection on a VDS layer of a straight line connecting the main vertex to the cluster position in ECAL. Consequently a gamma (γ) candidate can be defined requiring an anti-coincidence on the VDS layers [8]. The invariant mass distribution of electron/positron candidates obtained requiring two ECAL clusters with $P_t \geq 1.0$ GeV/c and a total energy $E_1 + E_2 \geq 15$ GeV is shown in Fig. 6. The superimposed dashed histogram corresponds to the γγ invariant mass distribution and is used to estimate the background. The distributions have been normalized in the regions $2.2 < m < 2.7$ GeV/c^2 and $m > 3.5$ GeV/c^2. As expected the prominent π^0 and η peaks in the γγ distribution are completely absent in the electron/positron one. Moreover the photon background spectrum seems to reproduce quite well the shape of the electron/positron distribution. The difference of the two distribution is shown in the lower part of the figure with a clear peak in the J/ψ position. The width of the peak is $\sigma \sim 185$ MeV/c^2 and is compatible with the width expected with the present calibration precision.

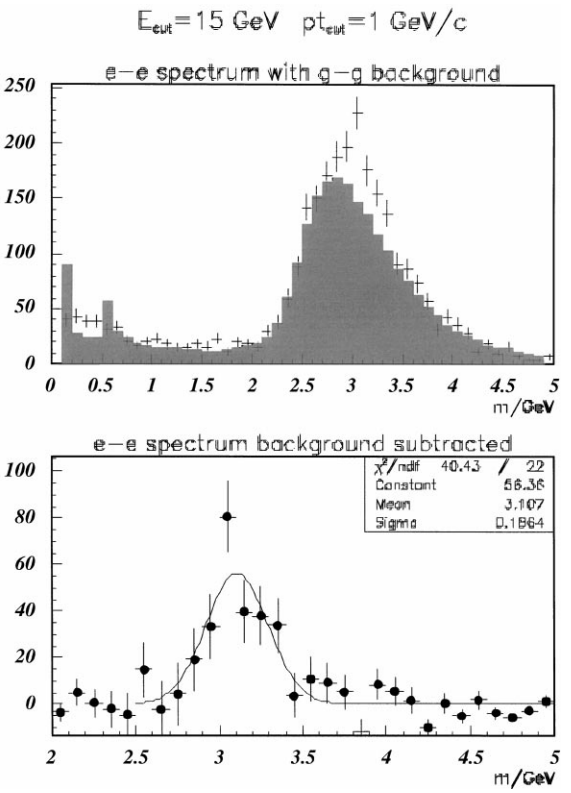

Fig. 6. Upper part: electron/positron invariant mass distribution requiring both clusters with $P_T > 1.0$ GeV/c and total energy $E_1 + E_2 \geq 15$ GeV. The dashed histogram is the γγ invariant mass distribution. Lower part: difference of the two distributions.

6. Conclusions

The HERA-B electromagnetic calorimeter has been designed to accomplish the stringent requirements of the HERA-B experiment. The detector together with the photomultiplier, the bases and the control electronics is installed in the experimental area. The readout and pretrigger electronics are in the production/installation phase and have been successfully tested. An iterative calibration procedure based on the π^0 detection has been set up reaching easily a calibration accuracy better than 5%. Besides the first physics signals like π^0, η and ω particles a clear J/ψ signal has been detected showing the functionality and good performances of the calorimeter and of the rest of the detector.

References

[1] T. Lohse et al., HERA-B: Proposal, DESY-PRC 94/02, 1994.
[2] E. Hartouni et al., HERA-B: Design Report, DESY-PRC 95/01, 1995.
[3] G.S. Atoyan et al., Nucl. Instr. and Meth. A 320 (1992) 144.
[4] A. Zoccoli et al., Proceeding of the VI Conference on Calorimetry in HEP, Frascati Physics Series, Vol. VI, pp. 817-826.
[5] B. Giacobbe et al., Proceedings of the VII Conference on Calorimetry in HEP, Tucson, Arizona, World Scientific Singapore, 1997, pp. 429–438.
[6] V. Alberico et al., Nuovo Cimento 110A (12) (1997) 1453.
[7] M. Villa et al. Proceedings of the VII Conference on Calorimetry in HEP, Tucson, Arizona, World Scientific, Singapore, 1997, pp. 537-546.
[8] M. Schmelling, Evidence for Heavy Flavours in the '99 Magnet-Off Data, HERA-B note 99-176, Physics 99-037.